Thermophoresis/diffusion as a plausible mechanism for unipolar resistive switching in metal–oxide–metal memristors

Dmitri B. Strukov, Fabien Alibart & R. Stanley Williams

Applied Physics A
Materials Science & Processing

ISSN 0947-8396

Appl. Phys. A
DOI 10.1007/s00339-012-6902-x

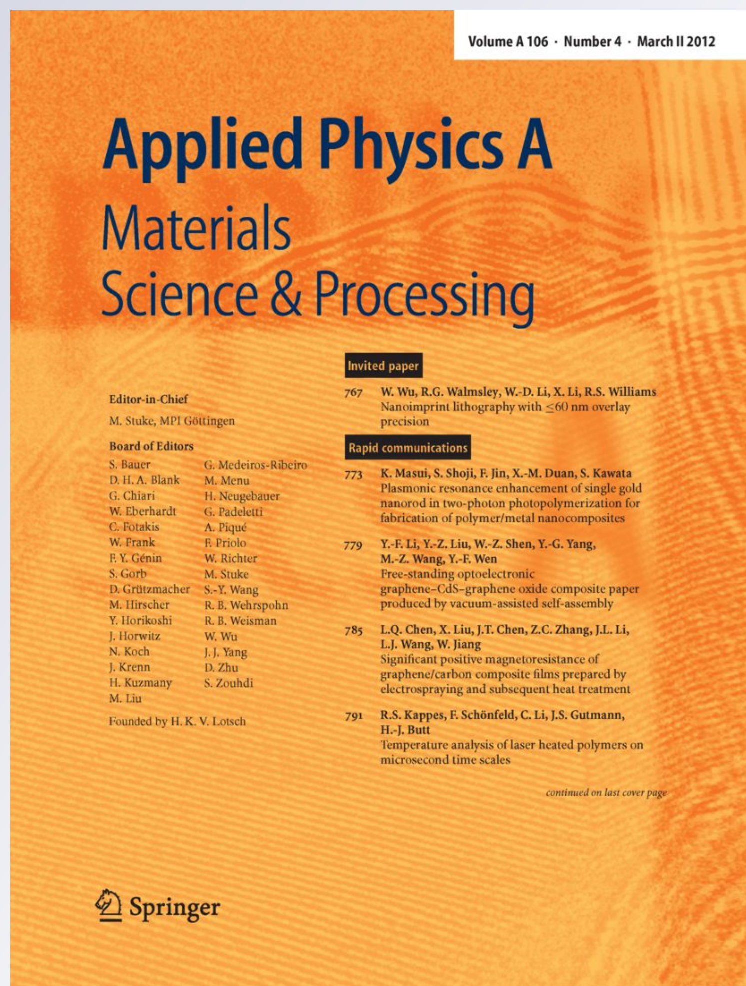

Volume A 106 · Number 4 · March II 2012

Applied Physics A
Materials
Science & Processing

Editor-in-Chief
M. Stuke, MPI Göttingen

Board of Editors
S. Bauer, D. H. A. Blank, G. Chiari, W. Eberhardt, C. Fotakis, W. Frank, F. Y. Génin, S. Gorb, D. Grützmacher, M. Hirscher, Y. Horikoshi, J. Horwitz, N. Koch, J. Krenn, H. Kuzmany, M. Liu, G. Medeiros-Ribeiro, M. Menu, H. Neugebauer, G. Padeletti, A. Piqué, F. Priolo, W. Richter, M. Stuke, S.-Y. Wang, R. B. Wehrspohn, R. B. Weisman, W. Wu, J. J. Yang, D. Zhu, S. Zouhdi

Founded by H. K. V. Lotsch

Invited paper

767 W. Wu, R.G. Walmsley, W.-D. Li, X. Li, R.S. Williams
Nanoimprint lithography with ≤60 nm overlay precision

Rapid communications

773 K. Masui, S. Shoji, F. Jin, X.-M. Duan, S. Kawata
Plasmonic resonance enhancement of single gold nanorod in two-photon photopolymerization for fabrication of polymer/metal nanocomposites

779 Y.-F. Li, Y.-Z. Liu, W.-Z. Shen, Y.-G. Yang, M.-Z. Wang, Y.-F. Wen
Free-standing optoelectronic graphene–CdS–graphene oxide composite paper produced by vacuum-assisted self-assembly

785 L.Q. Chen, X. Liu, J.T. Chen, Z.C. Zhang, J.L. Li, L.J. Wang, W. Jiang
Significant positive magnetoresistance of graphene/carbon composite films prepared by electrospraying and subsequent heat treatment

791 R.S. Kappes, F. Schönfeld, C. Li, J.S. Gutmann, H.-J. Butt
Temperature analysis of laser heated polymers on microsecond time scales

continued on last cover page

Springer

Springer

Your article is protected by copyright and all rights are held exclusively by Springer-Verlag. This e-offprint is for personal use only and shall not be self-archived in electronic repositories. If you wish to self-archive your work, please use the accepted author's version for posting to your own website or your institution's repository. You may further deposit the accepted author's version on a funder's repository at a funder's request, provided it is not made publicly available until 12 months after publication.

Springer

Author's personal copy

Appl Phys A
DOI 10.1007/s00339-012-6902-x

Applied Physics A
Materials Science & Processing

INVITED PAPER

Thermophoresis/diffusion as a plausible mechanism for unipolar resistive switching in metal–oxide–metal memristors

Dmitri B. Strukov · Fabien Alibart · R. Stanley Williams

Received: 19 March 2012 / Accepted: 21 March 2012
© Springer-Verlag 2012

Abstract We show that the SET operation of a unipolar memristor could be explained by thermophoresis, or the Soret effect, which is the diffusion of atoms, ions or vacancies in a steep temperature gradient. This mechanism explains the observed resistance switching via conducting channel formation and dissolution reported for TiO_2 and other metal-oxide-based unipolar resistance switches. Depending on the temperature profile in a device, dilute vacancies can preferentially diffuse radially inward toward higher temperatures caused by the Joule heating of an electronic current to essentially condense and form a conducting channel. The RESET operation occurs via radial diffusion of vacancies away from the channel when the temperature is elevated but the gradient is small.

1 Introduction

Nonvolatile resistive switching in metal–oxide–metal (MOM) devices has been studied for almost 50 years, see e.g. extensive reviews in Refs. [1–5], with the first observation in thin films reported in 1962 [6]. Two limiting forms of such switching have been recognized: bipolar, for which the switching back and forth from low resistance (SET) to high resistance (RESET) states requires opposite-polarity voltages applied across the device, and unipolar, for which SET and RESET are accomplished by applying different magnitudes of either polarity across the device [3, 5]. The same materials (e.g. TiO_2) can be used for both types of devices, and in fact individual devices have been observed to display both types of switching phenomena [7, 8]. Bipolar switches were recently identified [9] as examples of the original definition of the memristor [10], with the switching mechanism being electric field induced (and often thermally assisted) drift/diffusion of positively charged oxygen vacancies, which act as dopants, into and out of a thin layer of semiconductor to modulate its resistance [11, 12].

The mechanism for unipolar switching should be closely related to that for bipolar switching and, for example, several papers explain the RESET process [13–15] as temperature-activated diffusion that dissolves or breaks the conducting channel in the device. The fact that there is significant heating during both SET and RESET transitions is now well supported by numerous direct and indirect observations. For example, Joule heating during switching has been experimentally observed in both bipolar and unipolar devices by obtaining an infrared thermal map [16], thermometry of the internal switching region [17, 18] and the electrodes [19, 20], observation of thermally driven crystallization of as-fabricated amorphous films [21] and from coupled electrothermal simulations [19, 22, 23]. The fact that switching occurs at an elevated temperature explains the large retention-to-write-time ratio (the so-called write-time/retention dilemma [12, 24–26]) that is routinely observed in metal oxide devices.

However, to date there have not been any atomic-level mechanisms proposed that can explain the SET operation of unipolar switching consistently—only phenomenological models of various types [14, 15, 27–31]. In principle, pure drift/diffusion might explain unipolar switching when a multi-filament model is assumed. For example, one sequence of SET and RESET sweeps could result in the

D.B. Strukov (✉) · F. Alibart
Department of Electrical and Computer Engineering, University of California Santa Barbara, Santa Barbara, CA 93106, USA
e-mail: strukov@ece.ucsb.edu

R. Stanley Williams
NanoElectronics Research Group, Hewlett-Packard Laboratories, Palo Alto, CA 94304, USA

Published online: 31 March 2012

Author's personal copy

growth and subsequent rupture/dissolution of a filament, with the following SET sweep enabling the growth of another filament, etc. Though behavior consistent with such a mechanism was observed in some experiments [32], it cannot explain switching in unipolar devices with a high endurance. The fact that the applied electric field always has the same polarity for unipolar switching means that drift must be negligible in devices with high endurance, since otherwise vacancies would collect at one of the electrodes of the device and limit the number of switching cycles.

Here we show that the plausible mechanism of unipolar switching is thermophoresis/diffusion (or Soret–Fick diffusion) of oxygen vacancies in the metal oxide [33–36]. We also present a unified model that can explain the coexistence of bipolar and unipolar switching in the same material. We note that unipolar switching fits within the original definition of a memristive system [37], which was intended to be the generalization of the memristor [10], but, in a recent tutorial, Chua [38] has recommended that the nomenclature be simplified by calling all resistive switches that display a 'pinched hysteresis loop' (*I*–*V* zero crossing) by the name memristor.

2 Unipolar switching model

Figure 1 shows simple diagrams that can be used to understand the three main factors that determine the local electrochemical potential for mobile species, i.e. the presence of a concentration gradient, an electric field (for ions) and/or a temperature gradient. The corresponding fluxes induced by these gradients in one dimension are (see Appendix A1 for rigorous derivation)

$$J_{\mathrm{Fick}} \approx -D_{\mathrm{V}} \mathrm{d}n_{\mathrm{V}}/\mathrm{d}x, \tag{1}$$

$$J_{\mathrm{drift}} \approx D_{\mathrm{V}} n_{\mathrm{V}} Eq/(k_{\mathrm{B}}T), \tag{2}$$

$$J_{\mathrm{Soret}} \approx -D_{\mathrm{V}} S_{\mathrm{V}} n_{\mathrm{V}} \mathrm{d}T/\mathrm{d}x, \tag{3}$$

where n_{V} and T are the density of vacancies and local temperature as a function of x, respectively, D_{V} is the position-dependent diffusion factor for the vacancies, given by the expression $D_{\mathrm{V}} = f_{\mathrm{esc}} a^2 \exp[-U_{\mathrm{A}}/(k_{\mathrm{B}}T)]$, E is the electric field and S_{V} is the Soret coefficient for vacancies. Within the diffusion factor, f_{esc} is the effective vibrational frequency of the vacancies within their confining potential wells, a and U_{A} are the distance and the energy barrier between the potential wells, respectively, and k_{B} is the Boltzmann constant. The magnitude of the Soret coefficient is often estimated using thermodynamic arguments, even though it is strictly a kinetic parameter [39]. The sign of S_{V} can be either positive or negative, depending on the nature of the species influenced by the temperature gradient and the host. A moment's reflection reveals that for vacancies, the sign of S_{V} must be negative, since vacancies will move toward the hotter region of a temperature gradient (they move counter to the oxygen anions, as shown in Fig. 1c). Thus, we use the following expression for the Soret coefficient for vacancies: $S_{\mathrm{V}} = -U_{\mathrm{A}}/(k_{\mathrm{B}}T^2)$. Note that the derivation of Eqs. (1) and (2) is straightforward and appears in Ref. [12]. Equation (3) is similar to the one derived in Ref. [40] if one assumes $Q^*/R = U_{\mathrm{A}}/k_{\mathrm{B}}$, where Q^* is the heat of transport for oxygen vacancies and R is the ideal gas constant. In addition, Eqs. (1) and (3) are functionally similar to the drift/diffusion equations for charged vacancies that we have used previously to model bipolar switching [11]. The axial force of a potential gradient acting on a positively charged vacancy is replaced in the present case by the Soret force of a radial temperature gradient. For charged defects and/or thinner films and thus large electric fields, the electrostatic force is the greater. However, for neutral defects (see Appendix A2 for the discussion of this assumption) and/or certain thermal geometries of the device (e.g. thicker films), a large radial temperature gradient can be created and the Soret effect can become the dominant factor influencing vacancy motion. The sign of the applied electrical field is not important for the Soret effect, and thus the switching that results is necessarily 'unipolar' or independent of applied voltage polarity.

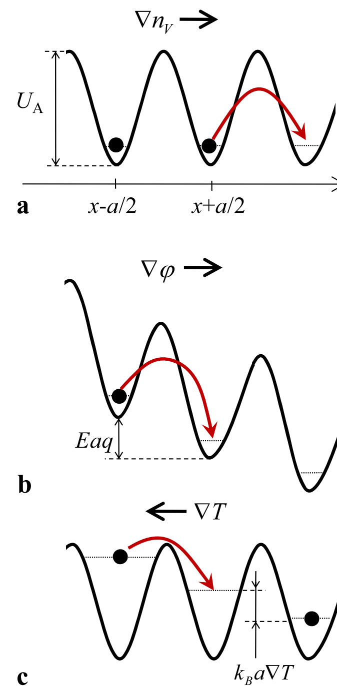

Fig. 1 Schematic illustration of the factors that influence oxygen anion motion for (**a**) Fick diffusion (concentration gradient), (**b**) drift (electrical potential gradient) and (**c**) thermophoresis (temperature gradient). The effective flux for oxygen vacancies is in the opposite direction of that for the anions

Figure 2 presents schematic illustrations of the unipolar SET transition for two different situations: essentially neu-

Author's personal copy

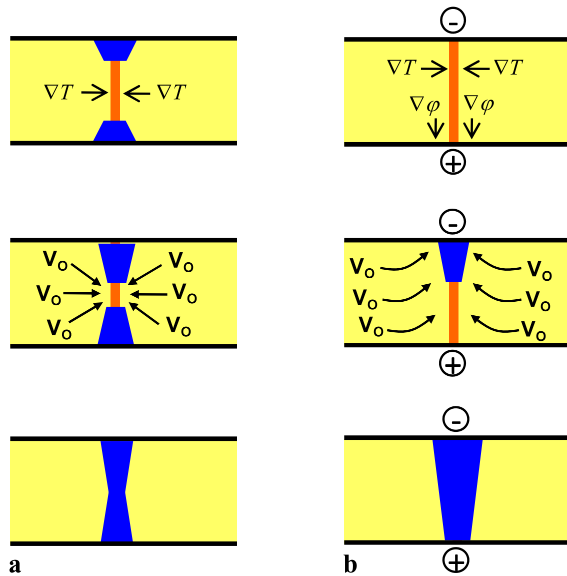

Fig. 2 Unipolar SET switching schematic illustrations for the side view of the device stack with: (**a**) neutral vacancies (symmetric channel formation) and (**b**) positively charged vacancies (asymmetric channel influenced by drift). The process is initiated in both cases by a purely electrical (threshold) transition that creates a radial temperature gradient in the film due to Joule heating. The Soret force attracts vacancies toward the electrical filament, and if the vacancies are positively charged they will be attracted toward the negative electrode

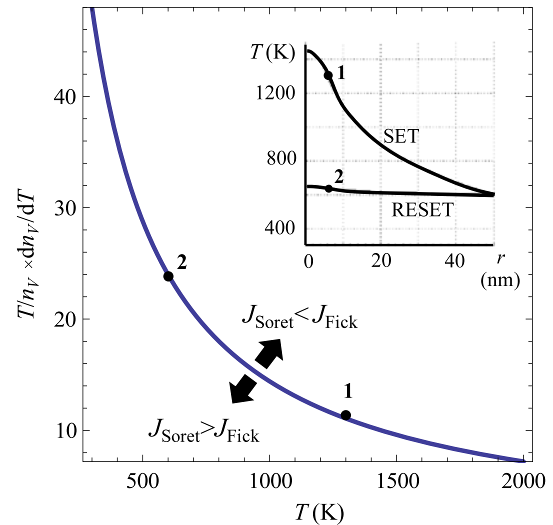

Fig. 3 The competition between Soret and Fick diffusion, illustrated by plotting the absolute value of $(dn_V/n_V)/(dT/T)$ vs. T with $U_A = 1.2$ eV for the case in which $|J_{Fick}| = |J_{Soret}|$. For conditions below the curve, the Soret effect dominates the vacancy transport. The *inset* shows the static radial temperature profiles that were used for modeling SET and RESET transitions using Eq. (6)

tral oxygen vacancies and charged vacancies that are subject to drift as well as thermophoresis. The abrupt onset of the SET transition is most likely due to a 'soft electrical breakdown' discussed by several authors [5, 41] that produces an electrical current filament and a significant radial temperature gradient because of Joule heating in the filament. The exact nature of the 'soft breakdown' is still debated, but it can be modeled by any S-type or current-controlled negative differential resistance. For example, a thermal instability [41, 42], an avalanche breakdown [43] or hot-electron effects [44] can all explain such behavior. The important point here is that the SET transition is essentially a two-step process: the first a purely electronic effect establishing the hot electrical filament and the second leading to a change in the material composition, i.e. the local vacancy concentration. The electrical filament is established in a very short time and results in a larger Joule heating and temperature gradient for the SET compared to the RESET process. A large thermal gradient is required for a purely unipolar SET process, but it also leads to rapid switching because of the high temperatures that exponentially increase the rate of activated processes.

The geometry and evolution of the metallic Ti_4O_7 filaments observed in TiO_2-based unipolar devices [45] can be understood in terms of the competition between the effects of the temperature and vacancy concentration gradients in the material. The Soret effect provides a means for attracting vacancies together to effectively condense and form a conducting channel in an oxide, and thus is responsible for the unipolar SET operation; if the vacancies are also influenced by drift the channels will have the truncated triangular shape [45] as illustrated in Fig. 2b. Outward radial Fick diffusion is responsible for the RESET transition, e.g. conductive channel dissolution. Both effects are always present and in opposition, so we need to examine the conditions under which the Soret effect can lead to a net increase in the concentration of vacancies. Taking the absolute value of the ratio of Eqs. (1) and (3) yields

$$|J_{Fick}/J_{Soret}| \approx \left|k_B T^2/(U_A n_V) \times dn_V/dT\right| = \left|k_B T/U_A \times (dn_V/n_V)/(dT/T)\right|, \quad (4)$$

which provides the conditions for when the Soret vacancy flux is larger in magnitude than the Fick diffusion flux: the product of the temperature gradient, which is normalized with respect to temperature, and the dimensionless factor $U_A/k_B T$ should be larger than the concentration gradient, which is also normalized with respect to concentration. The factor $U_A/k_B T$ is about 30 at room temperature and an activation energy of $U_A = 1.2$ eV (which would be required for nonvolatile memory effect [12, 26] and somewhat typical for oxygen vacancies in crystalline TiO_2 [46]) and decreases with increasing temperature. Figure 3 shows a plot of the factor $|dn_V/n_V)/(dT/T)|$ vs. T for the case in which $|J_{Fick}| = |J_{Soret}|$, and thus the boundary separating the conditions for which the device will SET or RESET.

In order to completely simulate this mechanism for unipolar switching, we would need to solve simultaneous

Author's personal copy

differential equations in three dimensions for the Soret, Fick and drift fluxes of vacancies, the drift/diffusion equations for electrons and holes, the Poisson equation for all the charged species and the heat equation. Rather than tackle this challenge here, we illustrate the plausibility of our theory by solving the Soret–Fick continuity equation in cylindrical coordinates:

$$\frac{\partial n_V}{\partial t} = -\left[\frac{U_A}{k_B}\frac{1}{r}\frac{\partial}{\partial r}\left(D_V r \frac{n_V}{T^2}\frac{\partial T}{\partial r}\right) - \frac{1}{r}\frac{\partial}{\partial r}\left(D_V r \frac{\partial n_V}{\partial r}\right)\right]. \tag{5}$$

Instead of using a time-dependent heat equation, we used the following temperature profiles for SET and RESET, shown in the inset of Fig. 3:

$$T(r) = T(R_O) + \left[T(R_F) - T(R_O)\right] \ln[R_O/r]/\ln[R_O/R_F], \quad R_F < r \le R_O, \tag{6}$$
$$T(r) = T(0) + \left[T(R_F) - T(0)\right] r^2/R_F^2, \quad r = R_F,$$

where Eq. (6) is the solution of the static heat equation in radial coordinates [23] and the boundary conditions were chosen to approximate experimental observations. For the particular solutions of Eq. (5) shown in Fig. 4, the radius of the conducting channel $R_F = 5$ nm, the outer channel radius $R_O = 50$ nm and, with $T(R_O) = 600$ K, $T(0) = 650$ K, $T(R_F) = 640$ K for RESET and $T(0) = 1450$ K, $T(R_F) = 1350$ K for SET. The maximum values of temperature chosen for the SET and RESET temperature profiles are close to previously reported analyses [18, 19, 23, 29]. The accuracy of these profiles has a high degree of uncertainty because of dynamical effects (e.g. the soft electrical breakdown may lead to a rapid discharge of the local junction capacitance and a transient spike in the heating rate of the oxide material) and the uncertainty in the initial electrical filament radius, but the fact that the internal temperature is significantly different for SET and RESET transitions will be demonstrated in the experimental section below.

For the transition to the SET state, the initial vacancy concentration was assumed to be uniform with $n_V(r) = 0.1 n_M$, where n_M is the critical vacancy concentration at which a transition from insulator to conductor occurs. Figure 4a shows snapshots of the vacancy concentration profile for exponentially increasing time steps normalized to the specific time τ at which the conducting filament radius (defined as the maximum value of the radius for which $n_V(r) > n_M$) reaches $0.1 R_O$. For the RESET transition calculations (Fig. 4b), the initial concentration profile was chosen to be that at time τ for the SET transition. The dimensionless units for concentration were chosen because Eq. (5) can be scaled by a constant, so it is convenient to express the concentration

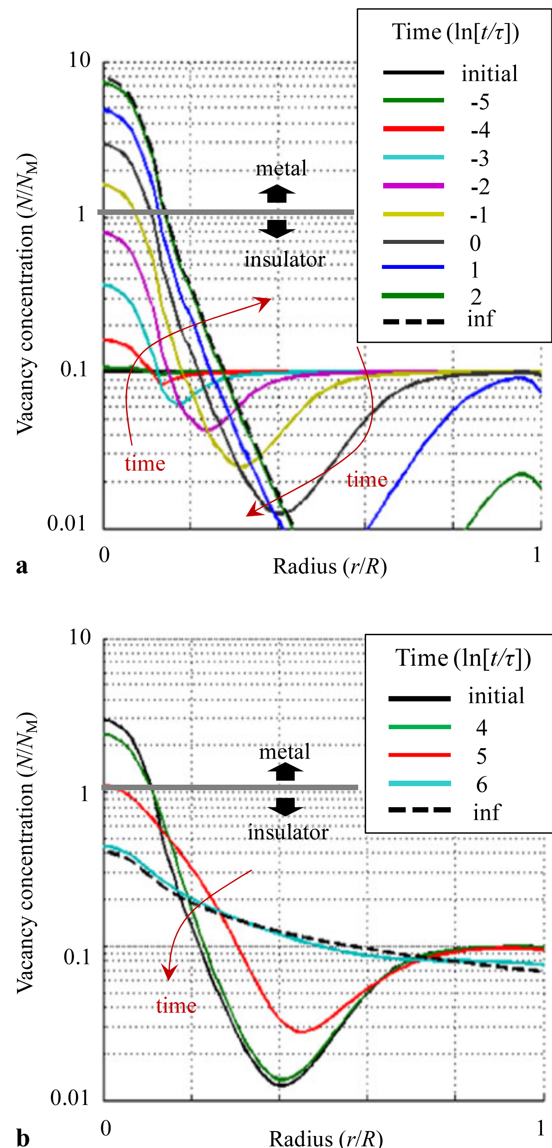

Fig. 4 Vacancy concentration profile evolution, shown for convenience in dimensionless units, determined by solving the radial Fick—Soret diffusion equations for (**a**) SET and (**b**) RESET transitions, using the constant-temperature profiles 1 and 2, respectively, from Fig. 3. The steady-state solutions, determined by fixed outer cylindrical boundary conditions, in both panels are shown with *dashed black lines*

in units of n_M. For example, $n_M = 5 \times 10^{21}$ cm^{-3} could correspond to the metallic Magnelli phase Ti_4O_7 [45]. On the other hand, the choice for dimensionless time was chosen to show the relative time steps with respect to the full SET time transition. While τ is a strong function of U_A, it cannot be factored from Eq. (6), and thus the simulation is specific for the cases with the temperature profiles shown in the inset of Fig. 3 and for $U_A = 1.2$ eV and $\tau = 10$ ms.

The simulation results in Fig. 4a clearly show the formation of a cylindrical region under SET conditions in which the vacancy concentration can reach a maximum value two

Author's personal copy

orders of magnitude larger than the background vacancy concentration, and thus form a highly conducting channel through the oxide film. In the simulation presented here, there were no attractive or repulsive interactions between the vacancies; if such forces had been present, there could have been a maximum value for the concentration that represents an effective condensed phase of vacancies in the oxide, such as a Magnelli phase in TiO_2. Under RESET conditions, shown in Fig. 4b, the channel dissolves as the vacancies diffuse laterally back outward into the matrix.

3 Experimental test

To test one of the major aspects of our theory, the influence of a temperature gradient, we performed a series of unipolar switching experiments with TiO_2 devices in which we studied the effect of an applied triangular voltage pulse duration on a device initially in the SET state. Figure 5a shows that the device behaved in the usual fashion for a unipolar switch with the alternating application of SET and RESET voltage sweeps. As Fig. 5b shows, longer triangular voltage pulses (4 s–2 ms) applied to a SET device induced a RESET transition, as expected. However, the effect of shorter pulses (200 µs–2 µs) was significantly different, and the device actually switched to a slightly lower resistance state for the shortest pulses.

To understand the effect of pulse duration on the temperature profile in a device, we compared the maximum power applied to the device when it RESET successfully (6.2 mW, 7.3 mW and 19.3 mW for the 4 s, 200 ms and 2 ms triangular voltage pulse widths, respectively) to that when it did not reset (72 mW in all three cases). Previous simulations have shown [19] that the peak internal temperature in a device reaches ~90 % of the maximum value, which is approximately proportional to the power ($I \times V$), within nanoseconds of the application of a voltage, but the area of the heated region increases with time, or essentially proportional to the total energy deposited in the device. We can thus understand why the RESET operation occurred at different voltages for the three triangular pulses: the slower the voltage increase of the triangular pulse, the more time is allowed for vacancies to diffuse from the conducting channel, and thus the internal temperature does not have to get as high for the longer pulses to dissolve the conducting channel. For the three shortest pulses, the maximum internal temperature spiked to a much higher value at the peak voltage of 3 V and there was not much time for the heated area to spread—thus the temperature gradient was much larger for these pulses and the Soret force not only kept the vacancy channel intact but even attracted more vacancies, as shown by the decrease in the resistance of the device for the 20-µs and 2-µs pulses. In order to show that the device had not become stuck in

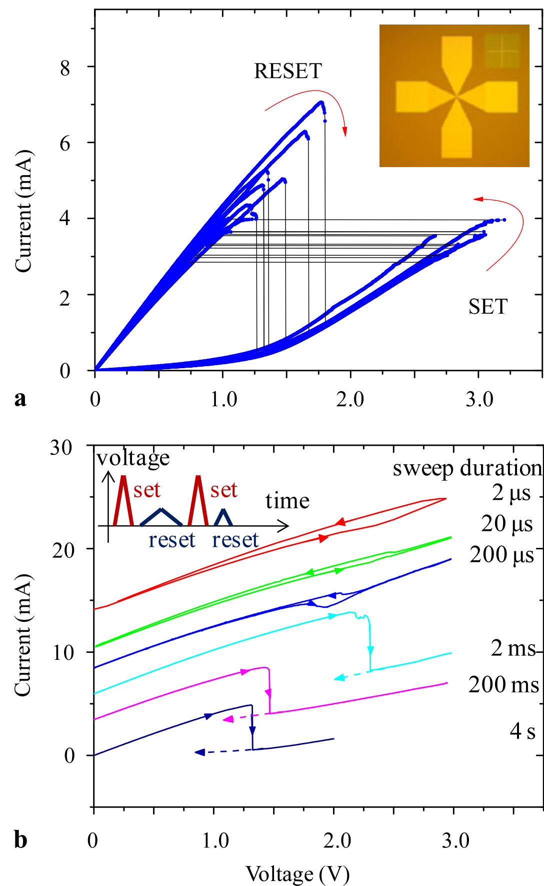

Fig. 5 Unipolar switching behavior in TiO_2: (**a**) SET and RESET transitions by applying the same bias protocol to the device shown in the inset, and (**b**) applying nominally RESET triangular voltage pulses with exponentially smaller duration (*inset*). The *I*–*V* curves are shifted along the *y* axis for convenience, but are otherwise drawn with the same scale. Each curve is labeled with the time duration of the pulse, with the bottom three curves having successfully RESET but the top three showing little influence of the applied pulse

the SET state after the application of a short pulse, it was successfully RESET at a lower voltage with a slower pulse.

4 Discussion

The pulse length experiments shown in Fig. 5b demonstrate an important issue: the switching in all memristors is dependent on the rate of change of one or more internal state variables [9, 10, 37] of the device. There are no purely threshold voltages or currents for switching—the apparent abrupt changes that are often observed in resistive switching are actually caused by nonlinear current–voltage characteristics, nonlinear dopant dynamics or both [47]. In the case of the unipolar switching results of Fig. 5a, the abrupt decrease and increase of the resistance can be understood by the fact that the vacancy concentration in the conducting channel either

Author's personal copy

exceeded or fell below, respectively, the concentration required for metallic conductivity. Thus, it is important to always perform experiments in which the time or rate dependence of switching is explicitly measured in order to expose the dynamical behavior of the device.

The use of static temperature profiles for analyzing SET and RESET transitions neglected the dependence of Joule heating in the device on local changes in electrical conductance, leakage currents and the cross-sectional area of the conducting channel (which changes with time). The latter effect was demonstrated to produce self acceleration during the RESET process [29]. However, the most important issue for our model is the fact that the thermal gradients are very different for SET and RESET transitions, which were illustrated in our pulsed switching experiments. The magnitude of the temperature defines the absolute time scale for the switching transition (together with the activation energy), whereas the scale of the temperature gradient in the device determines if the resistance will increase, decrease or stay the same.

A more complete picture of memristive switching in oxides must also include drift in the electrical potential gradient. The simultaneous presence and interplay of drift, thermophoresis and diffusion can explain the coexistence of unipolar and bipolar switching in a single device (e.g. Fig. 2b). Depending on the local chemical potential, i.e. the background doping and/or band bending, the mobile defects could be neutral or charged in the same material system, which can control whether the system is in the bipolar or unipolar switching regime. Moreover, the mechanism described for SET switching should be similar to the forming process of both bipolar and unipolar devices. For example, thermophoresis explains the observation of a conducting pillar in the center of a cylindrical hole in the oxide film of an electroformed TiO_2-based device after the top electrical contact has been peeled off [48]. During electroforming, vacancies are created by the drift of oxygen anions to the positive electrode, where they discharge and combine to form O_2. The resulting oxygen vacancies are drawn together to form the central pillar by the Soret force in the large radial temperature gradient created by the power expended during the electroforming process.

5 Experimental details

The top and bottom contacts for the TiO_2 devices had ‘dog bone’ structures to enable four-point-probe measurements. The resistance of the electrodes was measured to be $\sim$80 Ω, compared to the total resistance of the electrodes plus TiO_2 conducting channel of 200–300 Ω in the SET state. The active area of the device was 1 μm^2. An evaporated Ti/Pt bottom electrode (5 nm/35 nm) was patterned by conventional optical lithography on a Si/SiO_2 substrate (500 μm/200 nm, respectively). Then, a 60-nm TiO_2 switching layer was deposited by atomic layer deposition at 200 °C using titanium isopropoxide ($C_{12}H_{28}O_4Ti$) and water as reactants. A Pt/Au electrode (15 nm/25 nm) was evaporated on top of the TiO_2 blanket layer. Rapid annealing of the device was performed at 500°C in two passes, first with N_2 and then with a mixture of 80 % N_2 and 20 % O_2 at one atmosphere for 5 min to crystallize the TiO_2. The electrical measurements were performed with an Agilent B1500 parameter analyzer in ambient conditions. Each device was formed with a negative voltage sweep from 0 to −15 V (the forming voltage was around −14 V) and a current compliance of 360 μA. A few sweeps between 0 and 5 V were applied before obtaining a stable unipolar behavior of the device. The conventional unipolar switching *I–V* loops in Fig. 5a were measured using voltage control for the RESET transition and current control for the SET transition in quasi-DC mode (sweep time was around 4 s). The fast *I–V* measurements were acquired in a two-probe configuration using the waveform generator and measurement unit capability of the Agilent B1500 that allowed a sampling rate of 10 ns and a rise/fall time between 0 and 5 V of as low as 80 ns.

6 Conclusion

We proposed a mechanism for the SET operation and more generally the purely thermal nature of unipolar resistive switching. The theory was illustrated by the solution of the radial Soret–Fick diffusion equations to show both SET and RESET transitions and tested via a simple pulse-length-dependent experiment to examine how the switching dynamics responds to the internal temperature gradient caused by Joule heating. To the best of our knowledge, this is the first atomic-scale explanation for the unipolar SET transition and discussion of the full range of phenomena that control both unipolar and bipolar switching. This new model provides opportunities for engineering memristors by designing structures to have specified temperature gradients that tune the dynamical properties to match desired resistive switching characteristics.

Acknowledgements The work at UCSB was supported via NSF grant CCF-1028336.

Appendix A1: Derivation of Eqs. (1)–(3)

In the spirit of the microscopic hopping model [12, 26, 40, 49], we consider a one-dimensional billiard ball model with thermal, concentration and potential gradients and derive Eqs. (1)–(3) here to place them all on an equal footing.

Author's personal copy

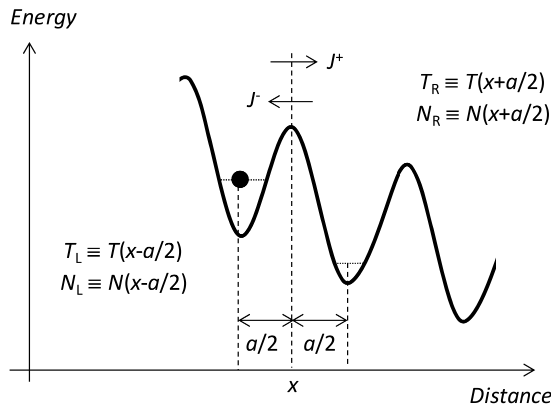

Fig. 6 Notation used for deriving Eqs. (1)–(3) for simplified billiard ball model

The ion fluxes in the positive (J^+) and negative (J^-) directions crossing an imaginary plane in the potential profile at position x (Fig. 6) are given by the following:

$$J^- = \frac{1}{2} a f N_R \exp\left[-\frac{U}{kT_R} - \frac{Eqa}{2kT_R}\right]\left(1 - \frac{N_L}{N_{MAX}}\right), \tag{7a}$$

$$J^+ = \frac{1}{2} a f N_L \exp\left[-\frac{U}{kT_L} + \frac{Eqa}{2kT_L}\right]\left(1 - \frac{N_R}{N_{MAX}}\right), \tag{7b}$$

$$J = J^+ - J^-, \tag{7c}$$

$$N_L = N - \frac{a}{2}\frac{dN}{dx}, \tag{8a}$$

$$N_R = N + \frac{a}{2}\frac{dN}{dx}, \tag{8b}$$

$$T_L = T - \frac{a}{2}\frac{dT}{dx}, \tag{9a}$$

$$T_R = T + \frac{a}{2}\frac{dT}{dx}. \tag{9b}$$

Here J is the total current, while N_R, N_L, T_R, T_L are the concentrations and temperatures on the right and on the left of the imaginary plane, respectively. Other notation is similar to that introduced in Sect. 2 of the paper. In this derivation, we use the ad hoc formula for the excluded volume effect (last term in Eqs. (7a) and (7b)), similar to Ref. [26].

Next, we simplify Eq. (7c) by deriving the first-order approximation (i.e. neglecting higher order terms) of Eqs. (7a)–(7c) and show that the current in this case can be decomposed into three independent terms—Soret, Fick and drift components (Eqs. (1)–(3) of the paper). In particular, combining Eqs. (7a, 7b, 7c)–(9a, 9b) together we obtain the following:

$$J = \frac{1}{2} af\left(N - \frac{a}{2}\frac{dN}{dx}\right)\exp[+]\left(1 - \frac{(N + \frac{a}{2}\frac{dN}{dx})}{N_{MAX}}\right) - \frac{1}{2} af\left(N + \frac{a}{2}\frac{dN}{dx}\right)\exp[-]\left(1 - \frac{(N - \frac{a}{2}\frac{dN}{dx})}{N_{MAX}}\right)$$
$$\approx \frac{1}{2} af N\left(\exp[+] - \exp[-]\right)\left(1 - \frac{1}{N_{MAX}}\right) - \frac{1}{4} a^2 f \frac{dN}{dx}\left(\exp[+] - \exp[-]\right), \tag{10}$$

where the approximation is due to the omission of the high-order terms and

$$\exp[-] \equiv \exp\left[-\frac{U}{kT_R} - \frac{Eqa}{2kT_R}\right] = \exp\left[-\frac{U}{k(T + \frac{adT}{2dx})} - \frac{Eqa}{2k(T + \frac{adT}{2dx})}\right], \tag{11a}$$

$$\exp[+] \equiv \exp\left[-\frac{U}{kT_L} + \frac{Eqa}{2kT_L}\right] = \exp\left[-\frac{U}{k(T - \frac{adT}{2dx})} + \frac{Eqa}{2k(T - \frac{adT}{2dx})}\right]. \tag{11b}$$

To further simplify Eq. (10), we define the $(\exp[+] \pm \exp[-])$ terms, i.e.

$$\exp[+] \pm \exp[-] = \exp\left[-\frac{U'}{1+\beta}\right]\exp\left[-\frac{W}{1+\beta}\right] \pm \exp\left[-\frac{U'}{1-\beta}\right]\exp\left[-\frac{W}{1-\beta}\right], \tag{12}$$

where for convenience we denote

$$U' \equiv \frac{U}{kT}, \tag{13a}$$

$$\beta \equiv \frac{a}{2T}\frac{dT}{dx}, \tag{13b}$$

$$W \equiv \frac{Eqa}{2kT}. \tag{13c}$$

Noting that $\beta \ll 1$ is always true for any practical range of thermal gradients and temperatures, we use Taylor's expansion about $\beta = 0$ so that

$$\exp\left[-\frac{U'}{1 \pm \beta}\right] \approx \exp[-U'] \pm \exp[-U']U'\beta, \tag{14a}$$

$$\exp\left[\pm\frac{W}{1+\beta}\right] \approx \exp[\pm W] + \exp[\pm W]W\beta. \tag{14b}$$

Therefore, substituting Eqs. (14a) ands (14b) into Eq. (12), we obtain

$$\exp[+] + \exp[-] \approx \exp[-U']\left(2\cosh[W] + 2W\beta\cosh[W] + 2U'\beta\sinh[W]\right), \tag{15a}$$

$$\exp[+] - \exp[-] \approx \exp[-U']\left(2\sinh[W] + 2W\beta\sinh[W] + 2U'\beta\cosh[W]\right), \tag{15b}$$

where the approximation sign is due to the omission of the higher order terms in β^2. Substituting Eqs. (15a) and (15b)

Author's personal copy

into Eq. (4), we obtain

$$J = \frac{2D}{a} N\big(\sinh[W] + W\beta \sinh[W] + U'\beta \cosh[W]\big) \times \left(1 - \frac{1}{N_{\mathrm{MAX}}}\right) - D\frac{\mathrm{d}N}{\mathrm{d}x}\big(\cosh[W] + W\beta \cosh[W] + U'\beta \sinh[W]\big), \tag{16}$$

where

$$D = \frac{1}{2} a^2 f \exp[-U'] \tag{17}$$

is a typical equation for thermally activated diffusion.

Equation (16) is the general form of the ionic current in the presence of thermal, concentration and potential gradients. For small electric fields, $W \ll 1$ so that $\sinh W \approx W$ and $\cosh W \approx 1$, and for sufficiently low concentrations $N \ll N_{\mathrm{MAX}}$. In this case, Eq. (16) simplifies to

$$J \approx \frac{2D}{a} N\big(W + U'\beta\big) - D\frac{\mathrm{d}N}{\mathrm{d}x} = \mu N E + DSN\frac{\mathrm{d}T}{\mathrm{d}x} - D\frac{\mathrm{d}N}{\mathrm{d}x}, \tag{18}$$

which corresponds to classical drift, Fick diffusion and thermophoresis, i.e. Eqs. (1)–() where

$$\mu \equiv \frac{qD}{kT}, \tag{19a}$$

$$S \equiv \frac{U}{kT^2} \tag{19b}$$

are ion mobility and Soret coefficient, respectively. Note that the approximation in Eq. (18) is due to the fact that $W^2\beta$ and $(1+U')W\beta$ are higher order terms and much smaller than the other terms. For example, $W^2\beta \ll U'\beta$ because of the small electric field assumption, so this term is much smaller than the thermophoresis current. Likewise, it is easy to show that $(1+U')W\beta \approx \frac{U}{kT}\frac{Eqa}{2kT}\frac{a}{2T}\frac{\mathrm{d}T}{\mathrm{d}x} \ll 1$.

Appendix A2: On the assumption of the neutrality of mobile defects

In our analysis for Fig. 2a, we assumed that mobile defects, i.e. oxygen vacancies, might be neutral so that we could neglect the drift of the charged defects in the electric field. The validity of this assumption largely depends on the position of energy levels of mobile defects inside the band gap. In titanium dioxide, some density functional theory calculations predicted very shallow (or even in the conduction band) electronic states induced by oxygen vacancies [50], while early experimental work [51] and other theoretical investigations predicted rather deep states, i.e. with

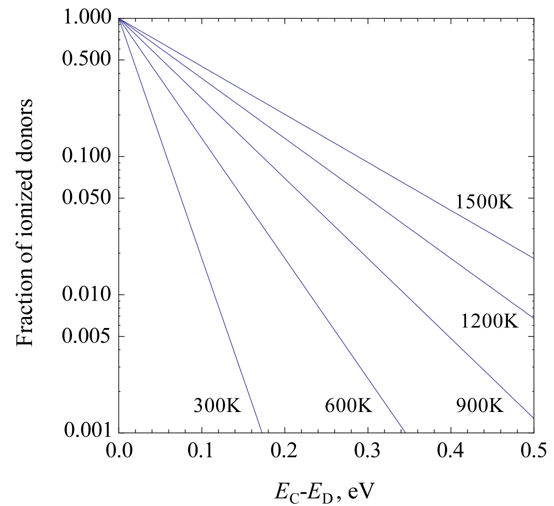

Fig. 7 Approximate fraction of ionized donors as a function of their energy levels for several temperatures

up to 1.1 eV for neutral vacancies, and high sensitivity on the morphology, nonstoichiometry and the presence of other dopants [52–55]. Similarly, relatively deep electronic states of ∼0.3 eV associated with oxygen vacancy defects are predicted for bulk NiO [56]. In the case of such deep energy levels, the neutrality assumption should be valid even for high temperatures. For example, Fig. 7 shows the fraction of ionized dopants as a function of the energy difference between the defects and the bottom of the conduction band for several values of temperature. Here we used simple Poisson–Boltzmann statistics to estimate the probability of the electron detachment to the conduction band, i.e.

$$\text{Fraction of ionized dopants} \approx \exp\big[-(E_{\mathrm{C}} - E_{\mathrm{D}})/k_{\mathrm{B}}T\big], \tag{20}$$

which is a good approximation for n-type materials with a large band gap.

Even if the neutrality assumption does not hold, the thermophoresis effect could still play the dominant role in defect transport given that the radial component of the electric field is much smaller than the axial component [57]. The switching dynamics, however, in that case will be most likely defined by the axial drift [31], similar to bipolar memristive devices—see Fig. 2b and its discussion.

References

1. G. Dearnaley, A.M. Stoneham, D.V. Morgan, Electrical phenomena in amorphous oxide films. Rep. Prog. Phys. **33**, 1129–1192 (1970)
2. H. Pagnia, N. Sotnik, Bistable switching in electroformed metal–insulator–metal devices. Phys. Status Solidi A **108**(11), 11–65 (1988)

Author's personal copy

3. A. Sawa, Resistive switching in transition metal oxides. Mater. Today **11**, 28–36 (2008)
4. K.K. Likharev, CMOL technology: devices, circuits, and architectures. J. Nanoelectron. Optoelectron. **3**, 203–230 (2008)
5. R. Waser, R. Dittman, G. Staikov, K. Szot, Redox-based resistive switching memories—nanoionic mechanisms, prospects, and challenges. Adv. Mater. **21**, 2632–2663 (2009)
6. M.T. Hickmott, Low-frequency negative resistance in thin anodic oxide films. J. Appl. Phys. **33**, 2669–2682 (1962)
7. D.S. Jeong, H. Schroeder, R. Waser, Coexistence of bipolar and unipolar resistive switching behaviors in a Pt/TiO_2/Pt stack. Electrochem. Solid-State Lett. **10**, G51–G53 (2007)
8. L. Goux, J.G. Lisoni, M. Jurczak, D.J. Wouters, L. Courtade, Ch. Muller, Coexistence of the bipolar and unipolar resistive-switching modes in NiO cells made by thermal oxidation of Ni layers. J. Appl. Phys. **107**, 024512 (2010)
9. D.B. Strukov, G.S. Snider, D.R. Stewart, R.S. Williams, The missing memristor found. Nature **453**, 80–83 (2008)
10. L.O. Chua, Memristor—the missing circuit element. IEEE Trans. Circuit Theory **18**, 507–519 (1971)
11. D.B. Strukov, J.L. Borghetti, R.S. Williams, Coupled ionic and electronic transport model of thin-film semiconductor memristive behavior. Small **5**(9), 1058–1063 (2009)
12. D.B. Strukov, R.S. Williams, Exponential ionic drift: Fast switching and low volatility of thin film memristors. Appl. Phys. A **94**(3), 515–519 (2009)
13. Y.-Y. Lin, F.-M. Lee, W.-C. Chien, Y.-C. Chen, K.-Y. Hsieh, C.-Y. Lu, A model for the RESET operation of electrochemical conducting bridge resistive memory (CB-ReRAM), in *Proc. Int. Electron Device Meet.*, San Francisco, CA, January 2010, pp. 22.2.1–22.2.4
14. F. Nardi, D. Ielmini, C. Cagli, S. Spiga, M. Fanciulli, L. Goux, D.J. Wouters, Control of filament size and reduction of reset current below 10 mA in NiO resistance switching memories. Solid-State Electron. **58**, 42–47 (2011)
15. D. Ielmini, F. Nardi, C. Cagli, Physical models of size-dependent nanofilament formation and rupture in NiO resistive switching memories. Nanotechnology **22**, 254022 (2011)
16. S.F. Karg, G.I. Meijer, J.G. Bednorz, C.T. Rettner, A.G. Schrott, E.A. Joseph, C.H. Lam, M. Janousch, U. Staub, F. La Mattina, S.F. Alvarado, D. Widmer, R. Stutz, U. Drechsler, D. Caimi, Transition-metal oxide-based resistance change memories. IBM J. Res. Dev. **52**(4–5), 481–492 (2008)
17. U. Russo, D. Ielmini, C. Cagli, A.L. Lacaita, S. Spigat, C. Wiemert, M. Peregot, M. Fanciulli, Conductive-filament switching analysis and self-accelerated thermal dissolution model for reset in NiO-based RRAM, in *Proc. Int. Electron Devices Meet.*, Baltimore, MD, December 2007, pp. 775–778, art. 4419062
18. J.L. Borghetti, D.M. Strukov, M.D. Pickett, J.J. Yang, R.S. Williams, Electrical transport and thermometry of electroformed titanium dioxide memristive switches. J. Appl. Phys. **106**, 124504 (2009)
19. S.H. Chang, S.C. Chae, S.B. Lee, C. Liu, T.W. Noh, J.S. Lee, B. Kahng, J.H. Jang, M.Y. Kim, D.-W. Kim, C.U. Jung, Effects of heat dissipation on unipolar resistance switching in Pt/NiO/Pt capacitors. Appl. Phys. Lett. **92**, 183507 (2008)
20. A. Shkabko, M.H. Aguirre, I. Marozau, T. Lippert, A. Weidenkaff, Measurements of current-voltage-induced heating in the $Al/SrTiO_{3-x}N_y/Al$ memristor during electroformation and resistance switching. Appl. Phys. Lett. **95**, 152109 (2009)
21. J.P. Strachan, D.B. Strukov, J. Borghetti, J.J. Yang, G. Medeiros-Ribeiro, R.S. Williams, The switching location of a bipolar memristor: Chemical, thermal, and structural mapping. Nanotechnology **22**, 254015 (2011)
22. N.A. Tulina, V.V. Sirotkin, Electron instability in doped-manganites-based heterojunctions. Physica C, Supercond. **400**(3–4), 105–110 (2004)
23. D.B. Strukov, R.S. Williams, Intrinsic constrains on thermally-assisted memristive switching. Appl. Phys. A **102**, 851–855 (2011)
24. H. Schroeder, V. Zhirnov, R.K. Cavin, R. Waser, Voltage-time dilemma of pure electronic mechanisms in resistive switching memory cells. J. Appl. Phys. **107**(5), 054517 (2010)
25. V.V. Zhirnov, R.K. Cavin, S. Menzel, E. Linn, S. Schmelzer, D. Brauhaus, C. Schindler, R. Waser, Memory devices: energy-space-time tradeoffs. Proc. IEEE **98**(12), 2185–2200 (2010)
26. M. Noman, W. Jiang, P.A. Salvador, M. Skowronski, J.A. Bain, Computational investigations into the operating window for memristive devices based on homogeneous ionic motion. Appl. Phys. A **102**(4), 877–883 (2011)
27. S.C. Chae, J.S. Lee, S. Kim, S.B. Lee, S.H. Chang, C. Liu, B. Kahng, H. Shin, D.-W. Kim, C.U. Jung, S. Seo, M.-J. Lee, T.W. Noh, Random circuit breaker network model for unipolar switching. Adv. Mater. **20**, 1154–1159 (2008)
28. G. Bersuker, D.C. Gilmer, D. Veksler, J. Yum, H. Park, S. Lian, L. Vandelli, A. Padovanu, L. Larcher, K. McKenna, A. Shluger, V. Iglesias, M. Porti, W. Taylor, P.D. Kirsch, R. Jammy, Metal oxide RRAM switching mechanism based on conductive filament microscopic properties, in *Proc. Int. Electron Device Meet.*, San Francisco, CA, January 2010, pp. 19.6.1–19.6.4
29. S. Larentis, C. Cagli, F. Nardi, D. Ielmini, Filament diffusion model for simulating reset and retention processes in RRAM. Microelectron. Eng. **88**(7), 1119–1123 (2011)
30. S.B. Lee, J.S. Lee, S.H. Chang, H.K. Yoo, B.S. Kang, B. Kahng, M.-J. Lee, C.J. Kim, T.W. Noh, Interface-modified random circuit breaker network model applicable to both bipolar and unipolar resistance switching. Appl. Phys. Lett. **98**, 033502 (2011)
31. K.M. Kim, D.S. Jeong, C.S. Hwang, Nanofilamentary resistive switching in binary oxide systems; a review on the present status and outlook. Nanotechnology **22**, 254002 (2011)
32. R. Münstermann, J.J. Yang, J.P. Strachan, G. Medeiros-Reibeiro, R. Dittman, R. Waser, Morphological and electrical changes in TiO_2 memristive devices induced by electroforming and switching. Phys. Status Solidi, Rapid Res. Lett. **4**, 16–18 (2010)
33. I. Goldhirsch, D. Ronis, Theory of thermophoresis. I. General considerations and mode-coupling analysis. Phys. Rev. A **27**, 1616–1634 (1983)
34. F. Ewart, K. Lassmann, H. Matzke, L. Manes, A. Saunders, Oxygen potential measurements in irradiated mixed oxide fuel. J. Nucl. Mater. **124**, 44–55 (1984)
35. J. Janek, H. Timm, Thermal diffusion and Soret effect in (U, Me) $O^{2+\delta}$: the heat of transport of oxygen. J. Nucl. Mater. **255**, 116–127 (1998)
36. L.J.T.M. Kempers, A comprehensive thermodynamic theory of the Soret effect in a multicomponent gas, liquid, or solid. J. Chem. Phys. **115**, 6330–6341 (2001)
37. L.O. Chua, S.M. Kang, Memristive devices and systems. Proc. IEEE **64**, 209–223 (1976)
38. L.O. Chua, Resistance switching memories are memristors. Appl. Phys. A **102**, 765–783 (2011)
39. R.D. Astumian, Coupled transport at the nanoscale: the unreasonable effectiveness of equilibrium theory. Proc. Natl. Acad. Sci. USA **104**, 3–4 (2007)
40. H. Timm, J. Janek, On the Soret effect in binary nonstochiometric oxides—kinetic demixing of cuprite in a temperature gradient. Solid State Ion. **176**, 1131–1143 (2005)
41. A.S. Alexandrov, A.M. Bratkovsky, B. Bridle, S.E. Savel'ev, D.B. Strukov, R.S. Williams, Current-controlled negative differential resistance due to Joule heating in TiO_2. Appl. Phys. Lett. **99**, 202104 (2011)
42. T. Kaplan, D. Adler, Electrothermal switching in amorphous semiconductors. J. Non-Cryst. Solids **8–10**, 538–543 (1972)
43. S. Sze, *Physics of Semiconductor Devices*, 2nd edn. (Wiley-Interscience, New York, 1981)

Author's personal copy

44. D. Ielmini, Threshold switching mechanism by high-field energy gain in the hopping transport of chalcogenide glasses. Phys. Rev. B **78**, 035308 (2008)
45. D.-H. Kwon, K.M. Kim, J.H. Jang, J.M. Jeon, M.H. Lee, G.H. Kim, X.-S. Li, G.-S. Park, B. Lee, S. Han, M. Kim, C.S. Hwang, Atomic structure of conducting nanofilaments in TiO_2 resistive switching memory. Nat. Nanotechnol. **5**, 148–153 (2010)
46. H. Iddir, S. Ogut, P. Zapol, N.D. Browning, Energetics and diffusion of intrinsic surface and subsurface defects on anatase TiO_2 (101). Phys. Rev. B **75**, 073203 (2007)
47. M.D. Pickett, D.B. Strukov, J. Borghetti, J.J. Yang, G.S. Snider, D.R. Stewart, R.S. Williams, Switching dynamics in a titanium dioxide memristive device. J. Appl. Phys. **106**, 074508 (2009)
48. J.J. Yang, F. Miao, M.D. Pickett, D.A.A. Ohlberg, D.R. Stewart, C.N. Lau, R.S. Williams, The mechanism of electroforming of metal oxide memristive switches. Nanotechnology **20**, 215201 (2009)
49. N.F. Mott, R.W. Gurney, *Electronic Processes in Ionic Crystals* (Oxford University Press, New York, 1940)
50. E. Cho, S. Han, H.-S. Ahn, K.-R. Lee, S.K. Kim, C.S. Hwang, First-principles study of point defects in rutile TiO_{2-x}. Phys. Rev. B **73**, 193202 (2006)
51. D.C. Cronemeyer, Infrared absorption of reduced rutile TiO_2 single crystals. Phys. Rev. **113**(5), 1123–1226 (1959)
52. F.M. Hossain, G.E. Murch, L. Sheppard, J. Nowotny, Ab initio electronic structure calculation of oxygen vacancies in rutile titanium dioxide. Solid State Ion. **178**, 319–325 (2007)
53. M.M. Islam, T. Bredow, A. Gerson, Electronic properties of oxygen-deficient and aluminum-doped rutile TiO_2 from first principles. Phys. Rev. B **76**, 045217 (2007)
54. G. Mattioli, F. Filippone, P. Alippi, A.A. Bonapasta, *Ab initio* study of the electronic states induced by oxygen vacancies in rutil and anatase TiO_2. Phys. Rev. B **78**, 241201 (2008)
55. H. Kamisaka, T. Hitosugi, T. Suenaga, T. Hasegawa, K. Yamashita, Denisty functional theory based first-principle calculation of Nb-doped anatase TiO_2 and its interactions with oxygen vacancies and interstital oxygen. J. Chem. Phys. **131**, 034702 (2009)
56. S. Park, H.-S. Ahn, C.-K. Lee, H. Kim, H. Jin, H.-S. Lee, S. Seo, J. Yu, S. Han, Interaction and ordering of vacancy defects in NiO. Phys. Rev. B **77**, 134103 (2008)
57. X. Guo, C. Schindler, S. Menzel, R. Waser, Understanding the switching-off mechanism in Ag^+migration based resistively switching model systems. Appl. Phys. Lett. **91**, 133513 (2007)